

Spurious instabilities in multiangle simulations of collective flavor conversion

Srdjan Sarikas, David de Sousa Seixas and Georg Raffelt

Max-Planck-Institut für Physik (Werner-Heisenberg-Institut), Föhringer Ring 6, 80805 München, Germany

(Dated: November 16, 2012)

The dense neutrino flux streaming from a core-collapse supernova can undergo self-induced flavor conversion caused by neutrino-neutrino refraction. Numerical studies of these nonlinear effects are challenging because representing the neutrino radiation field by discrete energy and angle bins can easily lead to unphysical solutions. In particular, if the number of angle bins N_a is too small, flavor conversion begins too deep and produces completely spurious results. At the same time, $N_a = 1$ (single-angle approximation) can be a good proxy for the $N_a \rightarrow \infty$ limit. Based on a linearized stability analysis, we explain some of the puzzling effects of discrete angle distributions.

PACS numbers: 14.60.Pq, 97.60.Bw

I. INTRODUCTION

The almost freely streaming flux of neutrinos emitted from a collapsed supernova (SN) core starts at a radius of 10–30 km, depending on the explosion phase and the neutrino energies, and at a density of $10^{12-13} \text{ g cm}^{-3}$. In such conditions, neutrino refraction in matter is so large that the propagation eigenstates are almost identical to the weak interaction eigenstates, even though all neutrino mixing angles are relatively large. Despite this simple boundary condition, the subsequent neutrino flavor evolution is surprisingly complicated due to the nonlinear impact of neutrino-neutrino refraction [1, 2].

One major problem in understanding this phenomenon is that numerical studies are challenging. If the integration begins close to the neutrino-emitting region of the SN (the “neutrino sphere”), large oscillation frequencies caused by the matter effect require many time steps. Moreover, the neutrino radiation field must be represented in some numerical form, in practice a finite number of energy and angle bins. Thus far axial symmetry of the neutrino stream was always assumed, implying that there was only one angle variable. Even with this simplification, reliable results require a large-scale computing effort [3].

Far away from the SN core, for example for a detector on Earth, the angle distribution is irrelevant and good energy resolution is sufficient. In particular, one can study the sharp spectral features that self-induced flavor conversion can produce [1, 4–7]. Therefore, many studies used the single-angle approximation, i.e., all neutrinos are put in a single angle bin corresponding to emission at the neutrino sphere at one specific angle relative to the radial direction. The simplest assumption of radially emitted neutrinos is not possible because parallel-moving neutrinos do not provide a refractive effect on each other. We always represent the single-angle case by assuming neutrino emission at 45° at the neutrino sphere.

To go beyond single-angle studies, upgrading to a small number N_a of angular bins is not enough. Beginning with the earliest studies [1], all multiangle simulations were haunted by the same peculiar effect. Although simulations with a large number of angular bins ($N_a \rightarrow \infty$)

and those with just a single angle ($N_a = 1$) often provide similar results, simulations using a relatively small N_a lead to results completely different from the two limiting cases. The required N_a to avoid spurious solutions had completely eluded explanation. Depending on circumstances, a few tens of modes might be enough, whereas in other cases one needs thousands or more bins.

For a simple (“single-crossed” [7]) neutrino spectrum, which is relevant during the SN accretion phase, self-induced flavor conversion begins at a critical onset radius. If only neutrino-neutrino refraction is relevant, then at larger neutrino densities, close to the SN core, the system is stable (“sleeping top” phase [8, 9]). The onset radius turns out to be almost the same in the single-angle and many-angle limits. On the other hand, if $N_a > 1$ is too small, flavor conversion begins at a smaller radius (where higher neutrino densities dominate) and tends to cause kinematical decoherence among angle modes [10]. Similar spurious solutions appear also when the normal matter effect is important.

This situation is to be contrasted with the role of energy bins that can be chosen to the desired resolution without affecting the qualitative behavior. Notice that neutrino energies (or rather the vacuum oscillation frequencies) appear in the linear part of the Hamiltonian, responsible for the vacuum oscillations. The angle variables, on the other hand, appear in the neutrino-neutrino interaction part which is the source of nonlinear effects. In the single-angle multienergy case, the flavor evolution is described by a small number of collective variables (“ N -mode coherence”), independently of the number of energy bins [11–13]. The ultimate source for this simple behavior is the simplicity of the single-angle Hamiltonian which contains as many constants of the motion as variables and thus is integrable [12, 14]. If detailed energy resolution is not important, we can therefore study conceptual aspects of multiangle effects in the monochromatic approximation where we use only one energy bin for neutrinos and one for antineutrinos.

The observed flavor conversion effect in the case of few angle modes must begin with an instability, i.e., with a runaway flavor mode in the interacting neutrino system. Understanding self-induced flavor conversion based on a

linearized stability analysis was pioneered by Sawyer [15] and further developed by our group and collaborators [16, 17]. We here apply this technique to the “ N_a effect” and find that many puzzling numerical observations easily fall into place. The spectrum of runaway modes is indeed very different for “ $N_a = \text{few}$ ” from $N_a = 1$ and $N_a \rightarrow \infty$. Additionally, the two neutrino mass hierarchies show striking differences.

II. LINEARIZED STABILITY APPROACH

A. Equations of motion

Following earlier works [16, 17, 19], we describe the two-flavor neutrino field by energy- and angle-dependent 2×2 matrices $\Phi_{E,u}(r)$. Boldface characters denote matrices in flavor space. The diagonal $\Phi_{E,u}$ elements are the ordinary number fluxes $F_{E,u}^\alpha$ (flavor α) integrated over a sphere of radius r , with negative E for antineutrinos. Moreover, we use the “flavor isospin convention” where $F_{E,u}^\alpha < 0$ for antineutrinos ($E < 0$) and $F_{E,u}^\alpha > 0$ for neutrinos ($E > 0$).

The off-diagonal elements of $\Phi_{E,u}(r)$, which are initially very small, represent phase information caused by flavor oscillations. The flavor evolution follows from the Schrödinger-like equation [19]

$$i\partial_r \Phi_{E,u} = [\mathbf{H}_{E,u}, \Phi_{E,u}] \quad (1)$$

with the Hamiltonian matrix

$$\begin{aligned} \mathbf{H}_{E,u} = & \frac{1}{v_u} \left(\frac{\mathbf{M}^2}{2E} + \sqrt{2} G_F \mathbf{N}_\ell \right) \\ & + \frac{\sqrt{2} G_F}{4\pi r^2} \int_{-\infty}^{+\infty} dE' \int_0^1 du' \frac{1 - v_u v_{u'}}{v_u v_{u'}} \Phi_{E',u'}. \end{aligned} \quad (2)$$

The matrix \mathbf{M}^2 of neutrino mass squares causes vacuum flavor oscillations and that of net charged lepton densities $\mathbf{N}_\ell = \text{diag}(n_e - n_{\bar{e}}, n_\mu - n_{\bar{\mu}}, n_\tau - n_{\bar{\tau}})$ adds the matter effect. The third term provides neutrino-neutrino refraction. A neutrino radial velocity at radius r is $v_u = (1 - u R^2/r^2)^{1/2}$, where R is the radius of the neutrino sphere, at which we label the neutrino angle modes by their emission angle θ_R . Our angle variable u is then defined by $v_u|_{r=R} = \cos \theta_R = (1 - u)^{1/2}$, equivalent to $u = \sin^2 \theta_R$. The factor $1 - v_u v_{u'}$ comes from the current-current nature of the weak interaction and leads to multiangle effects. Moreover, v_u appears in the denominator because we follow the flavor evolution projected on the radial direction.

Next, we study the instability driven by the atmospheric Δm^2 and the mixing angle θ_{13} . In the relevant SN region, propagation eigenstates are almost identical with weak-interaction eigenstates unless self-induced flavor conversion occurs. This means that initially the off-diagonal elements of $\Phi_{E,u}$ are very small, justifying a linearized stability analysis, but otherwise we do not need a specific numerical value of the mixing angle.

We switch to the variable $\omega = \Delta m^2/2E$ which is much better suited to study flavor oscillation than energy itself. Finally, the flux matrices are written in the form

$$\Phi_{\omega,u} = \frac{\text{Tr} \Phi_{\omega,u}}{2} + \frac{F_{\omega,u}^e - F_{\omega,u}^x}{2} \begin{pmatrix} s_{\omega,u} & S_{\omega,u} \\ S_{\omega,u}^* & -s_{\omega,u} \end{pmatrix}, \quad (3)$$

where $F_{\omega,u}^e$ and $F_{\omega,u}^x$ are the flavor fluxes at the neutrino sphere. The flux summed over all flavors, $\text{Tr} \Phi_{\omega,u}$, is conserved in our free-streaming limit. The ν_e survival probability is $\frac{1}{2}[1 + s_{\omega,u}(r)]$ in terms of the “swap factor” $-1 \leq s_{\omega,u}(r) \leq 1$. The off-diagonal element $S_{\omega,u}$ is complex and $s_{\omega,u}^2 + |S_{\omega,u}|^2 = 1$.

We have formulated our equations so that, for $\Delta m^2 > 0$, they describe the inverted hierarchy (IH) of the two possible neutrino mass orderings. The normal hierarchy (NH) can be implemented with the substitution $\Delta m^2 \rightarrow -\Delta m^2$ or, equivalently, $\omega \rightarrow -\omega$.

B. Stability condition

The possible onset of self-induced flavor conversions is best described in terms of the complex numbers $S_{\omega,u}$ which are very small as long as neutrinos are in the eigenstates of the weak interaction in the presence of matter. The small-amplitude limit means $|S_{\omega,u}| \ll 1$ and to linear order $s_{\omega,u} = 1$. Assuming in addition a large distance from the source so that $1 - v_u \ll 1$, the evolution equation linearized in $S_{\omega,u}$ and in u is [16]

$$\begin{aligned} i\partial_r S_{\omega,u} = & (\omega + u\bar{\lambda}) S_{\omega,u} \\ & - \mu \int du' d\omega' (u + u') g_{\omega',u'} S_{\omega',u'}. \end{aligned} \quad (4)$$

Here, $g_{\omega,u}$ is the neutrino spectrum ($\omega < 0$ for antineutrinos) which we normalize to the antineutrino flux, i.e. $\int_{-\infty}^0 d\omega \int_0^1 du g_{\omega,u} = -1$. The “asymmetry” between neutrinos and antineutrinos is $\epsilon = \int d\omega du g_{\omega,u}$.

Refractive effects are encoded in the r -dependent parameters

$$\begin{aligned} \lambda = & \sqrt{2} G_F [n_e(r) - n_{\bar{e}}(r)] \frac{R^2}{2r^2}, \\ \mu = & \frac{\sqrt{2} G_F [F_{\bar{\nu}_e}(R) - F_{\bar{\nu}_x}(R)]}{4\pi r^2} \frac{R^2}{2r^2}, \end{aligned} \quad (5)$$

and often combined in $\bar{\lambda} = \lambda + \epsilon\mu$. The factor $R^2/2r^2$ means that only the multiangle impact of the neutrino-neutrino and matter effects are relevant for our stability analysis, not the densities themselves. We normalize the neutrino-neutrino interaction strength μ , and consequently the spectrum $g_{\omega,u}$, to the $\bar{\nu}_e - \bar{\nu}_x$ flux difference at a chosen radius R , the nominal neutrino sphere. Physical results do not depend on the choice of R .

Writing solutions of the linear differential equation, Eq. (4), in the form

$$S_{\omega,u} = Q_{\omega,u} e^{-i\Omega r} \quad (6)$$

with complex frequency $\Omega = \gamma + i\kappa$ and eigenvector $Q_{\omega,u}$ leads to the eigenvalue equation [16]

$$(\omega + u\bar{\lambda} - \Omega) Q_{\omega,u} = \mu \int du' d\omega' (u+u') g_{\omega',u'} Q_{\omega',u'}. \quad (7)$$

The right-hand side of this equation is a linear polynomial in u so that the eigenvector must have the form

$$Q_{\omega,u} = \frac{a + bu}{\omega + u\bar{\lambda} - \Omega}, \quad (8)$$

where a and b are complex numbers. The form of the eigenfunctions is that of a Möbius transformation in the complex plane. This means that for fixed u we have a circle parametrized by ω and for fixed ω a circle parametrized by u . The physical range $u \in (0, 1)$ then maps to a circular arc in the complex plane.

Following Ref. [16] we note that, after inserting Eq. (8) into Eq. (7), both sides are linear polynomials in u . Self-consistency requires

$$\begin{pmatrix} I_1 - 1 & I_2 \\ I_0 & I_1 - 1 \end{pmatrix} \begin{pmatrix} a \\ b \end{pmatrix} = 0, \quad (9)$$

where

$$I_n = \mu \int du d\omega \frac{u^n g_{\omega,u}}{\omega + u\bar{\lambda} - \Omega}. \quad (10)$$

In contrast with Ref. [16] we have included a factor μ in the integral to make I_n dimensionless.

Nontrivial solutions for a and b exist if the determinant of the matrix in Eq. (9) vanishes, implying

$$(I_1 - 1)^2 = I_0 I_2. \quad (11)$$

Changing the neutrino mass hierarchy from inverted to normal is simply achieved by the sign change $\omega \rightarrow -\omega$ in the denominator of the integrand of Eq. (10).

III. CONTINUUM VERSUS SINGLE ANGLE

A. Neutrino spectrum

We use the simplest nontrivial setup that allows us to study the role of discrete angle modes, i.e., we consider a neutrino flux streaming from a sphere at radius R that emits monochromatic fluxes of $\bar{\nu}_e$ and ν_e . The ν_e flux is taken to be $1 + \epsilon$ times the $\bar{\nu}_e$ flux, representing deleptonization. The chosen vacuum frequency for monochromatic neutrinos and antineutrinos $\pm\omega_0$ determines the frequency scale of the system. We simplify the calculations by choosing $\omega_0 = 1$ as the unit of measure for all other frequencies such as μ , λ , κ and γ .

The angle distribution is taken to be black-body-like; i.e., the neutrino sphere is taken to emit neutrinos

isotropically into space without limb darkening. This assumption corresponds to a box spectrum in the u variable of the form

$$B(u) = \begin{cases} 1 & \text{for } 0 \leq u \leq 1, \\ 0 & \text{otherwise.} \end{cases} \quad (12)$$

Therefore, overall we study the neutrino spectrum

$$g_{\omega,u} = [-\delta(-\omega_0 - \omega) + (1 + \epsilon)\delta(\omega_0 - \omega)] B(u). \quad (13)$$

B. Inverted-hierarchy solution

To solve for the eigenvalues Ω with the spectrum Eq. (13) one can perform the integrals I_n analytically, leading to expressions involving logarithms and the arctan function. It is then straightforward to solve Eq. (11) for the eigenvalues Ω numerically. In the absence of matter ($\lambda = 0$) and for $\epsilon = 1/2$ we find the ‘‘Continuum (IH)’’ growth rate $\kappa = \text{Im}(\Omega)$ shown in Fig. 1. The interacting neutrino stream is stable for μ above a critical value μ_2 and below another μ_1 .

It is instructive to compare this continuum result with the single-angle approximation where we replace the box spectrum with a single mode placed at its center: $B(u) \rightarrow \delta(1/2 - u)$. This example corresponds to the original ‘‘flavor pendulum’’ [8]. One can solve the eigenvalue equation explicitly and finds

$$\Omega = -\frac{\epsilon\mu}{2} \pm \sqrt{1 - (2 + \epsilon)\mu + \left(\frac{\epsilon\mu}{2}\right)^2}. \quad (14)$$

The solution has an imaginary part for μ between the values $\mu_{1,2} = (1 + \epsilon/2 \pm \sqrt{1 + \epsilon})^{-1}$. For $\epsilon = 1/2$ we find $\mu_{1,2} = 20 \pm 4\sqrt{24}$. The maximum growth rate and the corresponding μ value is

$$\kappa_{\max} = \frac{2\sqrt{1 + \epsilon}}{\epsilon} \quad \text{at} \quad \mu_{\max} = \frac{2(2 + \epsilon)}{\epsilon^2}. \quad (15)$$

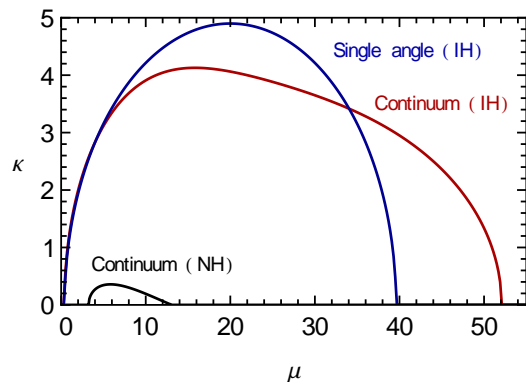


FIG. 1: Growth rate κ as a function of effective neutrino density μ in the absence of matter ($\lambda = 0$) and assuming $\epsilon = 1/2$. We show the single-angle and continuum cases for normal and inverted hierarchy.

For $\epsilon = 1/2$ we find $\kappa_{\max} = \sqrt{24}$ and $\mu_{\max} = 20$. In other words, while ω_0 is the only frequency scale in our problem and the dimensionless parameter ϵ is not especially small, the μ range where the system is unstable reaches to $\mu_2 \gg \omega_0$ and likewise, typical κ values are ω_0 times a significant numerical factor. A simple dimensional analysis could have suggested $\mu \sim \kappa \sim \omega_0$.

In Fig. 2 we show the continuum-case eigenfunctions $Q_{\omega,u}$ for $\omega = \pm 1$, assuming $\mu = 50$. As remarked earlier, $Q_{\omega,u}$ as a function of $0 \leq u \leq 1$ is a circular arc in the complex plane for fixed ω . We have normalized $Q_{\omega,u}$ so that the circle centers for different ω lie on a vertical line in the complex plane and the function $Q_{\omega=0,u}$ is a circle of unit radius.

The example in Fig. 2 is close to the upper instability range, i.e., roughly where neutrinos would start converting when the system evolves from high to low μ values in a SN. The angular modes remain fairly close to each other, corresponding to the observation that the multi-angle system evolves almost like the single-angle one.

As time goes on and the unstable mode grows exponentially, the system is described by an eigenvector such as the one shown in Fig. 2, independently of the initial condition. The evolution consists of an exponential growth with rate $\kappa = \text{Im}(\Omega)$ away from the origin in Fig. 2 and at the same time a precession around the origin with frequency $\gamma = \text{Re}(\Omega)$.

C. Normal-hierarchy solution

We next repeat this exercise for NH. Here, in the single-angle case, the system is always stable, as already known from the flavor pendulum [8]. However, in the multiangle

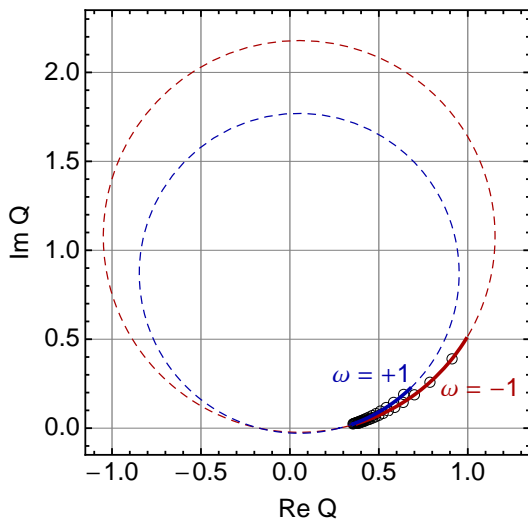


FIG. 2: Eigenfunction $Q_{\omega,u}$ for a box spectrum at $\mu = 50$. The solid arcs correspond to the physical range $0 \leq u \leq 1$. We also show as open circles an example for discrete angle eigenvectors with $N_a = 20$.

case the system does have instabilities [10]. In Fig. 1 we show the growth rate as a function of μ also for NH. The system is unstable only for a relatively small μ range and the instability parameter κ is an order of magnitude smaller than for IH.

Thus far we have ignored the ordinary matter effect. It can suppress self-induced flavor conversion [17–19], and this “multiangle matter effect” is particularly effective in suppressing the NH instability. Therefore, we continue to focus on the IH case.

IV. DISCRETE ANGLE MODES

A. Eigenvalue equation

We next turn to our main topic, the behavior of the system discretized in angle with $N_a > 1$ angle bins, and in energy with N_E energy bins. As we always consider both neutrinos and antineutrinos, the number of frequency bins is $N_\omega = 2N_E$. The spectrum is then implemented as

$$g_{\omega,u} = \sum_{i=1}^{N_\omega} \sum_{b=1}^{N_a} g_{i,b} \delta(\omega_i - \omega) \delta(u_b - u), \quad (16)$$

leading to

$$I_n = \mu \sum_{i=1}^{N_\omega} \sum_{b=1}^{N_a} \frac{u_b^n g_{i,b}}{\omega_i + u_b \bar{\lambda} - \Omega}. \quad (17)$$

One can then determine the eigenvalues Ω by solving Eq. (11) which amounts to finding the roots of a polynomial in Ω of order $N_\omega N_a$.

Alternatively, one can begin with the eigenvalue equation of Eq. (7) in discrete form

$$(\omega_k + u_c \bar{\lambda} - \Omega) Q_{k,c} = \mu \sum_{i=1}^{N_\omega} \sum_{b=1}^{N_a} (u_c + u_b) g_{i,b} Q_{i,b}. \quad (18)$$

This equation is of the form $(M - \Omega)Q = 0$ where Q is an $N_\omega N_a$ dimensional vector of complex numbers and M a $N_\omega N_a \times N_\omega N_a$ matrix. What remains is to find the eigenvalues Ω and eigenvectors Q_Ω of M . Both methods provide the same eigenvalues and eigenvectors.

B. Hair-comb spectrum

We will concentrate on the discrete monochromatic spectrum ($N_\omega = 2$) with N_a angle modes representing the original box spectrum in the form

$$B(u) \rightarrow H(u) = \frac{1}{N_a} \sum_{b=1}^{N_a} \delta\left(\frac{b-1/2}{N_a} - u\right). \quad (19)$$

For $N_a = 1$ this is our previous single-angle case and for $N_a \rightarrow \infty$ we expect to recover the continuum limit.

We can solve the discrete version of the eigenvalue equation in Mathematica without problem and we show the spectrum of growth rates in Fig. 3.

We always find the “ordinary mode” which, for large N_a , approaches the continuum solution (red dashed line in Fig. 3). In addition, we find $N_a - 1$ “extraordinary modes”, which arise at larger μ . With increasing N_a , the extraordinary modes shift their instability regions to larger μ values and, in the limit $N_a \rightarrow \infty$, disappear at infinity. Of course, for any finite N_a , the extraordinary modes exist at a sufficiently large μ .

In numerical studies, the neutrino flavor content is evolved along the radial SN direction, from large to small μ values. A numerical integration must begin at a depth where the ordinary mode is stable, i.e., to the right of the red dashed curve in Fig. 3. Inevitably, the system first encounters the extraordinary instabilities, leading to spurious solutions. Therefore, for a chosen inner boundary radius r_0 , the number of angle modes N_a must be large enough so that the extraordinary instabilities disappear to depths below it. If r_0 is chosen closer to the neutrinosphere, implying a larger μ , the required N_a is even larger. The most economical choice for the inner boundary radius r_0 is at the large- μ beginning of the ordinary instability region.

C. Nature of the extraordinary modes

The presence of more than one unstable mode is not surprising: solving Eq. (11) for a discrete case leads to a polynomial in Ω of order $2N_a$ and to equally many eigenvalues, some or all of which can have an imaginary part. However, empirically the extraordinary modes are quite distinct from the ordinary one.

One difference can be gleaned from the general form of the eigenvector $Q_{\omega,u}$, Eq. (8), and especially the resonance denominator $\omega + u\bar{\lambda} - \gamma - i\kappa$. Varying u between 0 and 1 over a continuous or discrete set of values may lead one to encounter a resonance of approximate width $\kappa/\bar{\lambda}$. We illustrate this point in Fig. 4 where we show an example for the modulus of $Q_{\omega,u}$ as a function of u ; the unshaded range corresponds to the physical range $0 \leq u \leq 1$. For the ordinary mode, the resonance lies in the unphysical range, implying that $|Q_{\omega,u}|$ does not vary much as a function of u . In other words, all angle modes are close to each other and evolve similar to the single-angle case. Avoiding the resonance is possible if the precession frequency is negative $\gamma < 0$, and this is indeed the case for the ordinary (or quasi-single-angle) mode.

The extraordinary modes, on the other hand, always seem to have $\gamma > 0$, i.e., they all precess in the opposite direction. The resonance falls in the physical u range and one or a few angle modes have $|Q_{\omega,u}|$ much larger than the others. In a plot of the circular arcs as in Fig. 2, the ordinary mode for $0 \leq u \leq 1$ traces out a small part of the circle, but the extraordinary ones trace most of

the circle. For our hair-comb spectra, the width of the resonance as a function of u has the approximate width

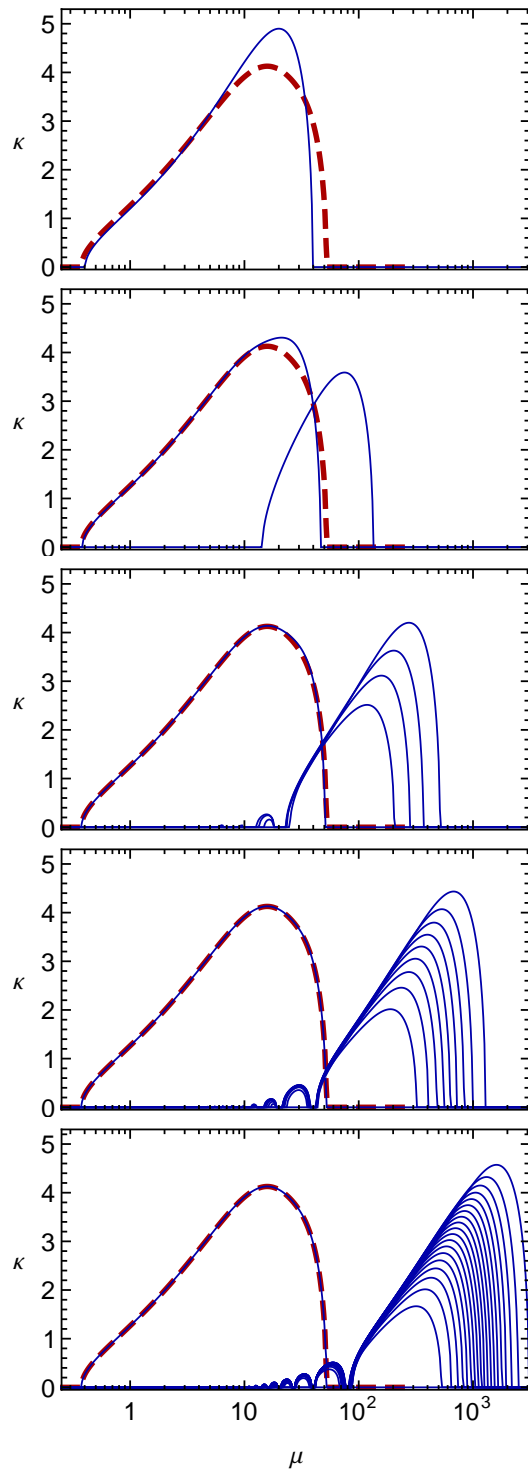


FIG. 3: Growth rates for unstable modes of the hair-comb spectrum in inverted hierarchy without matter ($\lambda = 0$) and $\epsilon = 1/2$. The number of angle modes is $N_a = 1, 2, 5, 10$ and 20 (top to bottom). As a red dashed line we show the continuum case. The top panel corresponds to Fig. 1.

of the spacing of the discrete u modes; i.e., typically one or two angle modes are on resonance. The different extraordinary modes differ in the angle mode that is on resonance. By their very nature, these modes are not quasi-single-angle and it is unsurprising that, when they have grown beyond the linearized regime, they tend to cause kinematical decoherence among angle modes.

We stress that, as far as the stability analysis is concerned, going beyond one energy bin (two frequencies) is not necessary. Since the equations of motion, Eq. (4), are linear in frequency ω , an average frequency can represent the whole spectrum. A multienergy treatment does provide, of course, more eigenvalues with respect to the monochromatic study, but no additional complex ones. The number of possible unstable solutions is related to the number of “spectral crossings” [7]. The additional solutions introduced by additional energy bins are purely real, and as such have no importance in the stability analysis. A multienergy treatment is necessary only in simulations if one is to resolve spectral features.

D. Other cases of extraordinary modes

Extraordinary modes are not limited to discrete angle distributions. For example, a u spectrum consisting of two boxes (instead of two delta spikes) has one ordinary and one extraordinary mode. Two boxes are equivalent

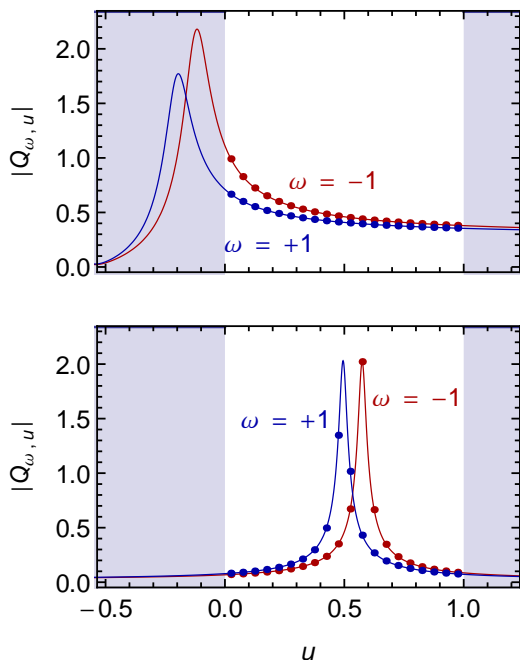


FIG. 4: Modulus of the eigenvector $Q_{\omega, u}$, according to Eq. (8), for $\mu = 50$ and the hair-comb angle distribution with $N_a = 20$. Only the range $0 \leq u \leq 1$ is physical. Top: Ordinary mode. Bottom: The extraordinary mode with the largest κ .

to a single box with a gap, and the μ range where the extraordinary mode appears migrates to larger μ values as the gap is chosen to be narrower. Likewise, if we consider two delta spikes with a separation Δu , then the solution for $\Delta u = 1/2$ corresponds to the upper panel of Fig. 3, $\Delta u = 0$ corresponds to the single-angle case, and for any other value one obtains two solutions, the extraordinary one migrating to higher μ values for decreasing Δu .

Generally it appears that “sharp features,” notably steps, in the angle spectrum cause extraordinary modes. (Of course we mean the following: extraordinary modes with nonvanishing growth rate $\kappa > 0$.) However, it happens only for the ascending steps (for increasing u), and not for the descending ones. For example, a descending staircase spectrum has only the ordinary (quasi-single-angle) mode, while an ascending one has as many extraordinary modes as steps minus 1. If the steps are somewhat smoothed, we still get the extraordinary modes. The location of the extraordinary mode on the μ axis depends on how narrow the spectral feature is, and the maximum κ depends on the magnitude of the jump.

A more mathematical classification of these observations is not available at present. In a realistic SN situation, the continuous angle spectrum is not a box, but typically a smoothly varying broad distribution. As such it should not have any extraordinary modes, or at least none with κ values comparable to the ordinary mode. In realistic numerical SN simulations, the appearance of extraordinary modes is probably caused only by a discretized angle spectrum.

V. MULTIANGLE MATTER SUPPRESSION

It is well known that a large density of matter, represented by the parameter λ , strongly modifies the instability in a multiangle treatment [17–21]. This “multiangle matter effect” does not appear in the single-angle case and is one important motivation to go beyond single-angle studies in the first place. Typically, nonvanishing growth rates appear only for $\mu \sim \lambda$ [16, 17]. In other words, for $\mu \lesssim \lambda$ the instability is suppressed and collective flavor conversion may not occur, notably during the accretion phase [17, 18].

To understand the impact of matter in the context of a discrete angle spectrum, we consider once more a box spectrum of angles. In Fig. 5 we show, as a red dashed line, the growth rate for different values of λ . We see that indeed the low- μ instability is suppressed and that the instability region is shifted to $\mu \sim \lambda$.

In addition, we show the solutions for a hair-comb representation with $N_a = 20$. For the extraordinary modes, the presence of λ has somewhat the opposite effect of enhancing the growth rates at low μ values. In the bottom panel of Fig. 5 we see that the ordinary mode disappears in the forest of extraordinary ones. In other words, in the presence of matter one needs a yet larger value for N_a to shift these modes away.

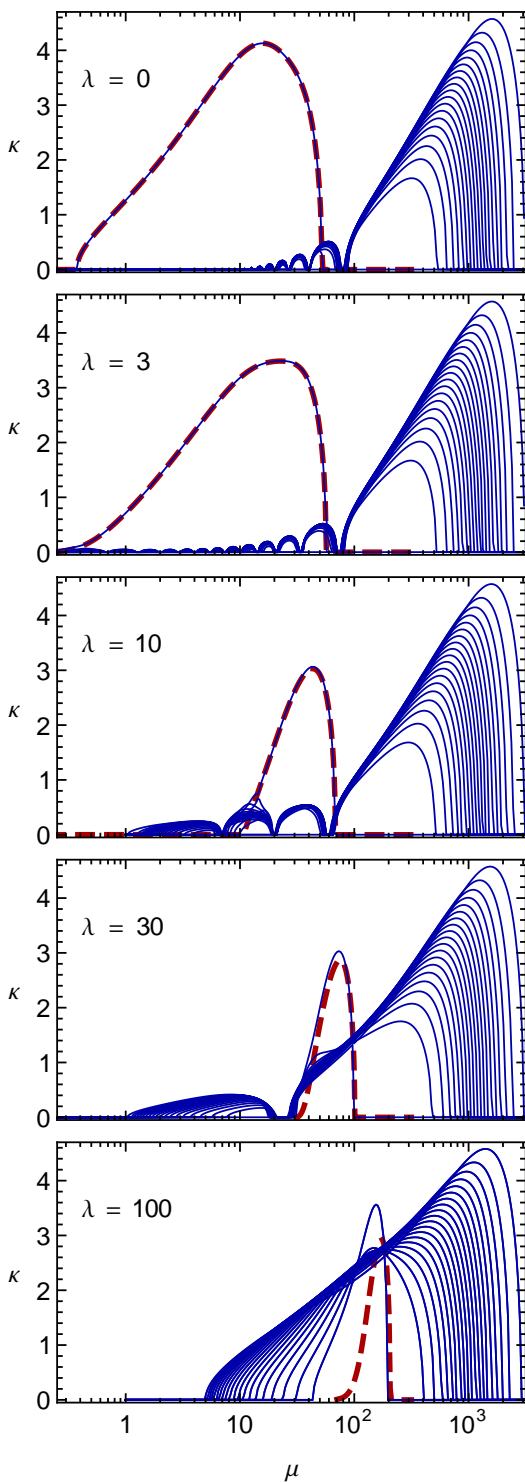


FIG. 5: Growth rates using the indicated values λ for the matter effect. Red dashed line: Continuous box spectrum for angles. Blue solid lines: Hair-comb representation with $N_a = 20$.

VI. DISCUSSION

We have used the method of linearized stability analysis to shed light on the appearance of spurious solutions in numerical studies of nonlinear neutrino flavor evolution. Spurious solutions appear when the neutrino radiation field is represented by discrete modes and the number of angles N_a is too small. The physical solution tends to be one where the angle modes remain nearly aligned (quasi single angle) and which we have called the ordinary mode. In addition, extraordinary modes appear at values of the effective neutrino density μ that depends on the spacing of the discrete modes. If they are sufficiently densely spaced, the extraordinary modes are at large μ (small SN radius) such that they do not spoil a numerical multiangle simulation.

The linear stability approach allows one to determine, without much effort, the growth rate of the physical instability as a function of the SN radius. Any instability is important only if the growth rate is large enough to take the system into the nonlinear regime on the available length scale. In a SN core, the effective neutrino and matter densities vary as power laws so that the relevant length scales correspond approximately to r . Typical growth rates κ are a few times the vacuum oscillation frequency ω_0 . For SN neutrino oscillations driven by the atmospheric mass difference, typically we have $\omega_0 \sim 0.5 \text{ km}^{-1}$ and so typical κ values are few inverse kilometers. The available length scales are tens to hundreds of kilometers, so the physical instability has enough time to become nonlinear, in agreement with numerical studies. Of course, the number of e -foldings required for a mode to become nonlinear depends on its initial amplitude.

In principle, then, for a concrete numerical example it is enough to find $\kappa(r)$ for the physical mode, based on a continuous angle distribution, and in this way find the onset radius of the instability. It would be enough to start the numerical integration at that radius. Since the starting point of flavor conversions is an exponential runaway, nothing is gained by starting deeper, i.e., in the stable regime of the ordinary mode. The number of angle modes then has to be chosen large enough that the growth rate of the extraordinary modes is much smaller than that of the ordinary one in the onset region. Starting the integration at a smaller radius requires enough angle modes to avoid the extraordinary modes becoming nonlinear before the system has reached the physical onset radius.

If one determines the required N_a by trial and error for a given numerical example, it has been observed that the solution becomes reproducible for N_a above some critical value, and nothing much changes by choosing N_a yet larger. This behavior corresponds to the aforementioned requirement that the extraordinary modes must not become nonlinear before the physical onset radius. The solution then no longer changes because, at the onset radius, the system will always select the physical eigenvec-

tor from whichever configuration the neutrino ensemble is in, by subjecting it to the exponential growth that will allow it to dominate the final outcome.

The appearance of unphysical modes in the discretized problem suggests that one is using a bad representation of the physical system. It would be desirable to cast the original equations of motion in a form that allows for a numerical treatment while avoiding spurious solutions.

Instead of using discrete angles one may consider spherical harmonics [22]. We have attempted this approach, truncating the expansion at some multipole order. Nevertheless, we obtain similar extraordinary modes and the required number of polynomials corresponds approximately to the required number of discrete angles. It remains to be seen whether a suitable closure of the multipole equations of motion can be found that avoids unphysical solutions without going to very high multipole order. Conversely, if this is not possible, it would be important to understand whether extraordinary modes are unavoidable in any scheme that fails to resolve suffi-

ciently fine details of the angle distribution.

For now the question remains open if numerical brute force is the only way forward to understand SN neutrino flavor evolution in more general situations beyond the toy models that have been studied thus far, or if the equations can be set up in a way that avoids the need for excessive computer power.

Acknowledgements

This work was partly supported by the Deutsche Forschungsgemeinschaft under Grant No. EXC-153 (Cluster of Excellence “Origin and Structure of the universe”) and by the European Union under Grant No. PITN-GA-2011-289442 (FP7 Initial Training Network “Invisibles”). D.S. acknowledges support by the Fundação para a Ciência e Tecnologia (Portugal).

-
- [1] H. Duan, G. M. Fuller, J. Carlson and Y.-Z. Qian, *Phys. Rev. D* **74**, 105014 (2006).
 - [2] H. Duan, G. M. Fuller and Y.-Z. Qian, *Annu. Rev. Nucl. Part. Sci.* **60**, 569 (2010).
 - [3] H. Duan, G. M. Fuller and J. Carlson, *Comput. Sci. Dis.* **1**, 015007 (2008).
 - [4] G. Raffelt and A. Yu. Smirnov, *Phys. Rev. D* **76**, 081301 (2007); **77**, 029903(E) (2008); *Phys. Rev. D* **76**, 125008 (2007).
 - [5] H. Duan, G. M. Fuller and Y.-Z. Qian, *Phys. Rev. D* **76**, 085013 (2007).
 - [6] G. L. Fogli, E. Lisi, A. Marrone and A. Mirizzi, *J. Cosmol. Astropart. Phys.* **12** (2007) 010. G. L. Fogli, E. Lisi, A. Marrone, A. Mirizzi and I. Tamborra, *Phys. Rev. D* **78**, 097301 (2008).
 - [7] B. Dasgupta, A. Dighe, G. Raffelt and A. Yu. Smirnov, *Phys. Rev. Lett.* **103**, 051105 (2009).
 - [8] S. Hannestad, G. Raffelt, G. Sigl and Y. Y. Wong, *Phys. Rev. D* **74**, 105010 (2006); **76**, 029901(E) (2007).
 - [9] H. Duan, G. M. Fuller, J. Carlson and Y.-Z. Qian, *Phys. Rev. D* **75**, 125005 (2007).
 - [10] A. Esteban-Pretel, S. Pastor, R. Tomàs, G. G. Raffelt and G. Sigl, *Phys. Rev. D* **76**, 125018 (2007).
 - [11] G. G. Raffelt and I. Tamborra, *Phys. Rev. D* **82**, 125004 (2010).
 - [12] G. G. Raffelt, *Phys. Rev. D* **83**, 105022 (2011).
 - [13] E. A. Yuzbashyan, *Phys. Rev. B* **78**, 184507 (2008).
 - [14] Y. Pehlivan, A. B. Balantekin, T. Kajino and T. Yoshida, *Phys. Rev. D* **84**, 065008 (2011).
 - [15] R. F. Sawyer, *Phys. Rev. D* **79**, 105003 (2009).
 - [16] A. Banerjee, A. Dighe and G. Raffelt, *Phys. Rev. D* **84**, 053013 (2011).
 - [17] S. Sarikas, G. G. Raffelt, L. Hüdepohl and H.-T. Janka, *Phys. Rev. Lett.* **108**, 061101 (2012). S. Sarikas and G. Raffelt, arXiv:1110.5572. S. Sarikas, I. Tamborra, G. Raffelt, L. Hüdepohl and H.-T. Janka, *Phys. Rev. D* **85**, 113007 (2012).
 - [18] S. Chakraborty, T. Fischer, A. Mirizzi, N. Saviano and R. Tomàs, *Phys. Rev. D* **84**, 025002 (2011); *Phys. Rev. Lett.* **107**, 151101 (2011). N. Saviano, S. Chakraborty, T. Fischer and A. Mirizzi, *Phys. Rev. D* **85**, 113002 (2012).
 - [19] A. Esteban-Pretel, A. Mirizzi, S. Pastor, R. Tomàs, G. G. Raffelt, P. D. Serpico and G. Sigl, *Phys. Rev. D* **78**, 085012 (2008).
 - [20] G. G. Raffelt, *Phys. Rev. D* **78**, 125015 (2008).
 - [21] H. Duan and A. Friedland, *Phys. Rev. Lett.* **106**, 091101 (2011).
 - [22] G. G. Raffelt and G. Sigl, *Phys. Rev. D* **75**, 083002 (2007).